UCID-18574-84-3



# MATERIALS PHYSICS QUARTERLY REPORT

## H DIVISION

## JULY THROUGH SEPTEMBER 1984

## FEBRUARY 1985

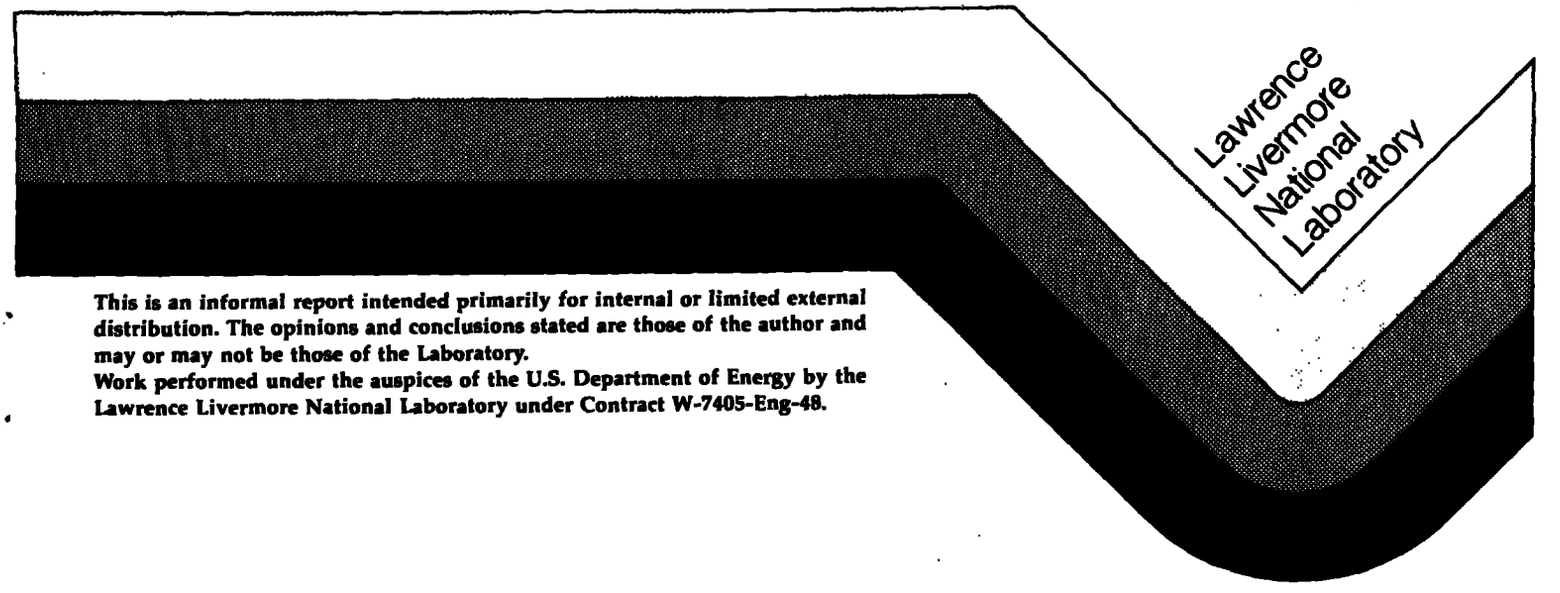



Work performed under the auspices of the U.S. Department of Energy by the Lawrence Livermore National Laboratory under Contract W-7405-Eng-48.

Printed in the United States of America
Available from
National Technical Information Service
U.S. Department of Commerce
5285 Port Royal Road
Springfield, VA 22161
Price: Printed Copy $ ; Microfiche $4.50

| Page Range | Domestic Price | Page Range | Domestic Price |
|---|---|---|---|
| 001-025 | $ 7.00 | 326-350 | $ 26.50 |
| 026-050 | 8.50 | 351-375 | 28.00 |
| 051-075 | 10.00 | 376-400 | 29.50 |
| 076-100 | 11.50 | 401-426 | 31.00 |
| 101-125 | 13.00 | 427-450 | 32.50 |
| 126-150 | 14.50 | 451-475 | 34.00 |
| 151-175 | 16.00 | 476-500 | 35.50 |
| 176-200 | 17.50 | 501-525 | 37.00 |
| 201-225 | 19.00 | 526-550 | 38.50 |
| 226-250 | 20.50 | 551-575 | 40.00 |
| 251-275 | 22.00 | 576-600 | 41.50 |
| 276-300 | 23.50 | 601-up[1] | |
| 301-325 | 25.00 | | |

[1]Add 1.50 for each additional 25 page increment, or portion thereof from 601 pages up.

CONTENTS

---

For comments or questions about this report, please contact the editor, John A. Moriarty (ext. 2-9964), or the individual authors.

## CONDENSED MATTER EXPERIMENT

### SHOCK COMPRESSION OF LIQUID HELIUM TO 56 GPa (560 KBAR)

W. J. Nellis, N. C. Holmes, A. C. Mitchell, R. J. Trainor, G. K. Governo, M. Ross, and D. A. Young

- Liquid He at 4.3 K and 1 atm was shocked to 16 GPa and 12 000 K and double shocked to 56 GPa and 21 000 K. Liquid perturbation theory has been used to determine an effective interatomic potential from which the equation of state of He can be obtained over a wide range of densities and temperatures.

We present shock-wave data for liquid He that has been compressed to densities up to 0.7 g/cm$^3$, five times greater than the normal liquid, and heated to temperatures up to 21 000 K. The maximum pressure attained is 56 GPa (560 kbar). These are the first shock data ever reported for liquid He and the conditions attained are more extreme than any achieved in other experiments. The highest static pressure so far attained in He is 16 GPa on the melting curve.[1]

The equation of state and intermolecular potential for dense He and $H_2$ have been widely studied because they are the simplest and most abundant of the elements. Their properties are important for modeling the giant planets where they are the major constituents and are subjected to pressures up to 4.5 TPa (45 Mbar) and temperatures up to 20 000 K in Jupiter and to about 1 TPa and 14 000 K in Saturn.[2] Saturn is of particular interest because studies have suggested that it has an internal energy source that is associated with unmixing and gravitational separation of the hydrogen-helium fluid at pressures below 1 TPa.[2] The existence of this phase transition depends very sensitively on the hydrogen and helium equations of state. In a series of recent papers we have reported shock-wave data[3] and theoretical calculations[4] for liquid $D_2$ shock-compressed to 76 GPa and 7000 K. This report summarizes the results of a similar study for He.

Strong shock waves were generated by the impact of planar projectiles into cryogenic specimen holders. Projectiles were accelerated to velocities

of 3-7 km/s by means of a two-stage light-gas gun.[5,6] Shock pressure, density, and specific internal energy were derived from the measured impactor velocity, shock velocity, and initial liquid density by means of the Hugoniot equations. The He specimens were initially in the liquid state at 4.3 K. The specimen holders[7,8] and coolant fill system[3] were similar to that used for liquid $H_2$. Several refinements were necessary to adapt the cryogenic design for He. The specimen holder was made from pure Al for improved thermal coupling between the liquid He coolant and the specimen cavity. The sample cavity was filled by condensing He gas by flowing the gas through a heat-exchange coil located in the coolant chamber. More than 100 layers of aluminized Mylar were wrapped on the assembly for thermal radiation shielding. The impact surface, which could not be covered, was an infrared mirror, diamond-turned and Au-plated for high reflectivity. A liquid $N_2$-cooled radiation shield was positioned in front of the impact surface to shield thermal radiation from all directions except the axis of the launch tube. Aluminum foil was contoured to the surrounding black inner wall of the gun target chamber. Specimen temperature was measured by a calibrated Ge resistance thermometer. Initial specimen density was liquid saturation density[9] at the measured temperature.

Our theoretical analysis combines a statistical-mechanical theory of liquids with an effective pair potential. The liquid theory used here is a modified hard-sphere variational perturbation theory.[10] We have tested the adequacy of various potentials and constructed one which fits the data optimally. Three useful potentials for comparison with data are: 1) molecular beam,[11] 2) Aziz, et al.,[12] and 3) linear muffin-tin-orbitals (LMTO).[13] The LMTO potential was derived from a pair potential fit to LMTO band structure calculations on solid He up to 25 TPa. The first two potentials are strictly two-body, but the third, is an effective potential which incorporates many-body effects. The LMTO and beam potentials are purely repulsive exponential functions. However, because of the very high temperatures along the Hugoniot, short-range repulsive contributions dominate, and the error due to omitting the attractive potential is negligible except at the lowest experimental point.

The theoretical curves are compared with experiment in Fig. 1. It is clear that the beam and Aziz potentials are too stiff, while the LMTO potential is somewhat too soft. These tendencies are strongly amplified in the calculation of the double-shock curves. This shows that many-body contributions to the effective potential have the effect of softening the two-body repulsion, and are very important in dense He. We have chosen an optimum potential with the same slope as the LMTO, but which has a larger pre-exponential coefficient. We find this potential to be $\phi(r) = 1.1 \cdot 10^5 \varepsilon \exp(-11r/r_m)$, where $\varepsilon/k$ = 10.8 K and $r_m$ = 2.9673 Å. For the highest experimental point on the principal Hugoniot, the liquid model predicts a temperature of approximately 12 000 K, and for the double-shock point, the prediction is approximatley 21 000 K.

In conclusion, the high densities and temperatures reached in the shock-wave experiments have determined the effective He pair potential in a previously unexplored region and confirm the importance of many-body effects. This potential can now be used to generate a He equation of state for the study of planetary interiors. Additional details on this work are available in the literature.[14]

## REFERENCES


1. P. Loubeyre, J. M. Besson, J. P. Pinceaux, and J-P. Hansen, Phys. Rev. Lett. 49, 1172 (1982).

2. D. J. Stevenson, Annu. Rev. Earth Planet. Sci. 10, 257 (1982).

3. W. J. Nellis, A. C. Mitchell, M. van Thiel, G. J. Devine, R. J. Trainor, and N. Brown, J. Chem. Phys. 79, 1480 (1983).

4. M. Ross, F. H. Ree, and D. A. Young, J. Chem. Phys. 79, 1487 (1983).

5. A. H. Jones, W. M. Isbell, and C. J. Maiden, J. Appl. Phys. 37, 3493 (1966).

6. A. C. Mitchell and W. J. Nellis, Rev. Sci. Instrum. 52, 347 (1981).

7. W. J. Nellis and A. C. Mitchell, J. Chem. Phys. 73, 6137 (1980).

8. W. J. Nellis, F. H. Ree, M. van Thiel, and A. C. Mitchell, J. Chem. Phys. 75, 3055 (1981).

9. R. D. McCarty, National Bureau of Standards Technical Note 631 (unpublished).

10. M. Ross, J. Chem. Phys. 71, 1567 (1979).

11. P. B. Foreman, P. K. Rol, and K. P. Coffin, J. Chem. Phys. 61, 1658 (1974).

12. R. A. Aziz, V. P. S. Nain, J. S. Carley, W. L. Taylor, and G. T. McConville, J. Chem. Phys. 70, 4330 (1979).

13. D. A. Young, A. K. McMahan, and M. Ross, Phys. Rev. B 24, 5119 (1981).

14. W. J. Nellis, N. C. Holmes, A. C. Mitchell, R. J. Trainor, G. K. Governo, M. Ross, and D. A. Young, Phys. Rev. Lett. 53, 1248 (1984).

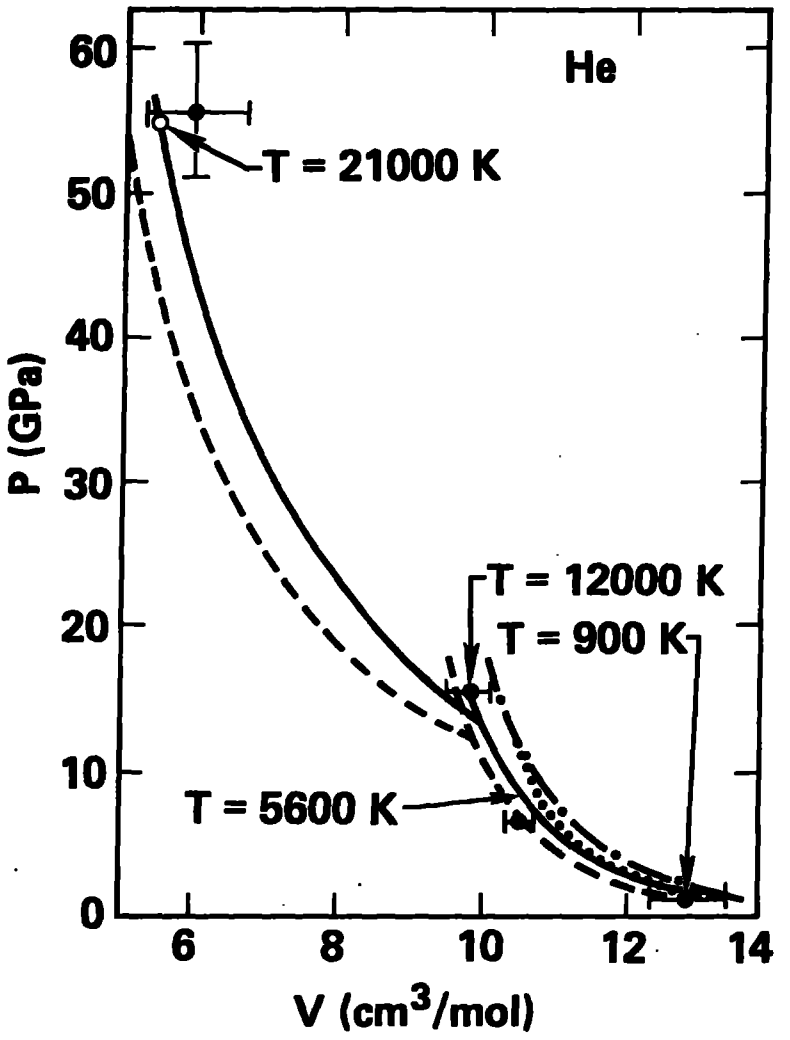


FIG. 1. Comparison of experimental (points with error bars) and theoretical (curves) helium Hugoniots. Calculations with four different pair potentials are compared with the single-shock data, but only the best two potentials are compared with the double-shock point. The solid curve was calculated using the optimized potential, the dashed curve with LMTO, the dots with Aziz, and the dot-dash with the beam potential. The open circle on the theoretical curve at 55 GPa is the double-shock point predicted by the theory for the experimental conditions (10 GPa = 100 kbar).

# RESHOCK HUGONIOT MEASUREMENTS ON ALUMINUM

G. R. Gathers

- Reshock measurements have been made on very pure aluminum samples using tantalum impactors and platinum anvils. Preliminary analysis shows the aluminum reached a compression of 2.3 and a pressure of 440 GPa.

Alt'shuler et al.[1] reported Hugoniot measurements on aluminum using conventional single shock waves generated by an iron impactor accelerated in a heavy lead cylinder by the combustion gases of explosives. The impactor reached a velocity of 8.64 km/s. The speed of both impactor and the shock wave were measured and used to determine Hugoniot parameters by the direct collision method. They reported a shock velocity $U_s$ of 12.94 km/s and particle velocity $U_p$ of 5.62 km/s. The aluminum reached a compression of 1.767 and a pressure of 197 GPa. The Gruneisen parameter was calculated using the Dugdale-McDonald relation and varied from an initial value of 2.1 to 1.3 for a pressure of 216 GPa and temperature 9670 K.

Reshock measurements have recently been made with the LLNL two-stage light-gas gun using tantalum impactors and platinum anvils to extend the available Hugoniot data closer to results available from the nuclear driver impedance match (NIM) measurements. Two shots were fired. The error range was larger than usual for gun shots both because of the reshock technique and because of the short interval times involved in the measurements. The interval time can be increased only by using thicker targets. The aspect ratio of the target must be preserved, however, to avoid systematic errors caused by release waves from the edges and the rear of the target. The available space in the gun does not permit this. The pin circles used in the targets were smaller than usual to avoid distortion of the impactor near its edges and the tantalum impactor was reduced in diameter to avoid distortion of the sabot near the walls of the gun barrel and to reduce the projectile mass, allowing higher velocities to be achieved.

Figure 1 shows the results. The principal Hugoniot of aluminum (based on fits to data below 200 GPa) is shown. The principal Hugoniot fit is reflected about the particle velocity of the first shock for each shot as an approximation to the reshock Hugoniot. The circles represent the results of the measurements with the experimentally measured shock velocity in the anvil. The squares correspond to the results of impedance matching the known Hugoniot of the anvil with the reflected Hugoniot of the baseplate obtained from previous fits at at lower pressures. The result of Alt'shuler et al.[1] is shown for comparison. Agreement between the impedance match and direct measurement is good for the second shot (TaAlPt2) but not for the first (TaAlPt1). Additional experiments are planned to resolve this discrepancy.

## REFERENCE

L.V. Alt'shuler, S. B. Kormer, A. A. Bakanova, and R. F. Trunin, Sov. Phys. JETP 11, (3), 573-579 (1960).

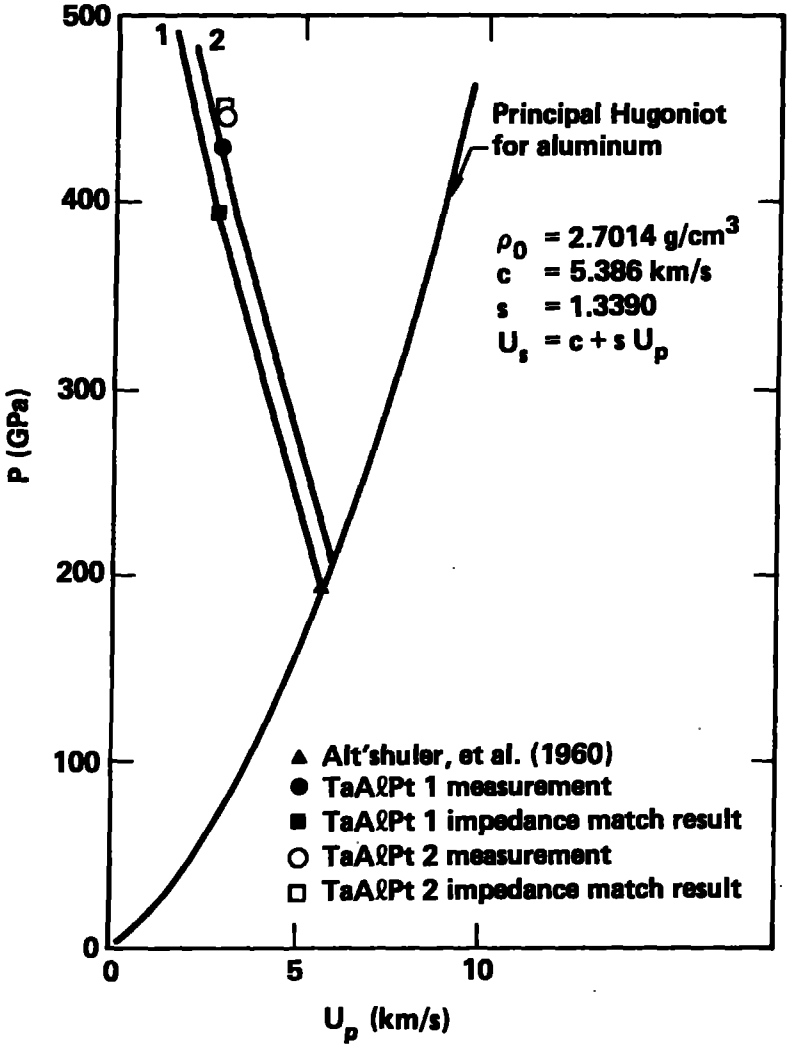


FIG. 1. Reshock results in aluminum. The principal Hugoniot obtained by fitting data for pressures below 200 GPa was reflected about the particle velocity produced by the initial shock to approximate the reshock Hugoniot for each shot (curves labeled 1 and 2).

## THEORY OF THE ALUMINUM SHOCK EQUATION OF STATE TO $10^4$ MBAR

D. A. Young

o New theoretical shock equations of state for aluminum are compared with experimental data, including new Soviet data to 4000 Mbar. Overall agreement is good, showing that current theoretical models of hot, dense matter are adequate. Significant electron shell structure effects are predicted in the 1000 Mbar region, but better experimental precision is needed for testing the models here.

A large mass of experimental shock Hugoniot data on aluminum below 100 Mbar has been accumulated in the past three decades,[1-7] and new Soviet experimental data to 4000 Mbar have recently been published.[8] At 4000 Mbar, Al is a weakly nonideal gas of electrons and nuclei. Thus, except for questions of experimental precision, the Hugoniot of Al has been fully explored in the sense that pressures above 4000 Mbar would only enter the theoretically uninteresting ideal gas region. Al is the first element for which such a complete collection of data is available.

Since Al is a simple nearly-free-electron metal, it is an ideal subject for theoretical calculations, and it has been proposed as a high pressure standard for shock-wave experiments.[9] Al is also an excellent material for exhibiting electron shell structure effects, since there are two filled shells (K and L) with widely separated ionization energies. It is, therefore, of interest to compare the whole range of experimental data with the best available theoretical models.

Despite a longstanding effort to generate a theoretical equation of state (EOS) model valid over a very wide range of temperature and density, we are still forced to use different models in different temperature-density regions. When a global EOS is needed, a table is constructed by connecting the various model EOS's together by interpolation.[10]

The P vs $\rho/\rho_0$ Hugoniot is shown in Fig. 1. Here the theoretical curve is compared with the available experimental data. Below a few Mbar the shock waves are produced with chemical explosives or a gas gun. Above this pressure, the energy source is a nuclear explosive. The uncertainties in the experimental EOS increase with pressure, and in the 1000 Mbar region they are very large.

As the Hugoniot pressure increases, shocked Al passes through a series of condensed matter regimes. Below P = 1.2 Mbar, Al is a solid. Above this pressure, Al passes through the two-phase melt region and into the liquid.[11] Above 20 Mbar, the thermal pressure is greater than the 0 K pressure, and the electron and nuclear thermal EOS contributions increase in importance. Above 76 Mbar, the temperature rises above the Fermi temperature, and the electron gas ceases to be nearly degenerate. Also in this region the electron-ion coupling becomes strong, and ionization of core electrons begins. Above 600 Mbar, because of the rising temperature, the electrons are once again weakly coupled to the ions. Above 5000 Mbar, core ionization is complete and Al has become a fully ionized, nearly ideal gas. Given the difficulty of modelling all of these regimes and the large errors in the experimental ultrahigh pressure EOS, the overall agreement between the tabular EOS and the experimental data is good.

A more detailed comparison of experiment with the tabular EOS and two other theoretical models in the maximum compression region is made in Fig. 2. ACTEX,[12] an ionization equilibrium plasma model, has been run to lower temperatures than used in constructing the EOS table, and density maxima due to electron shell structure are seen. The upper maximum is due to K-shell ionization, and the lower maximum to L-shell ionization. ACTEX theory becomes increasingly inaccurate in the L-shell region as the electron-ion interaction becomes comparable to kT, but at temperatures above this, it is the most rigorous theory available. INFERNO[13] is a self-consistent-field theory of atoms in plasmas which includes a treatment of bound states. The predicted Hugoniot also shows shell structure density maxima. No shell structure is seen in the TFNUC model because it uses a continuum model for the electron states. The core ionization region of the Hugoniot is clearly sensitive to

the approximations used in the model, as is shown in the difference between the ACTEX, INFERNO, and tabular EOS predictions.

It is clear from Fig. 2 that the experimental errors in the ultrahigh pressure data make it impossible to pick out detail which could be ascribed to shell structure, although the general density maximum is evident in the experimental points. A better comparison of theory and experiment awaits reduction of the experimental errors. However, the general adequacy of the models discussed here is not in doubt. This gives us confidence in applying these models to problems involving hot, dense, partially ionized fluids, such as stellar interiors, MHD fluids, and laser fusion plasmas.

## REFERENCES


1. A. C. Mitchell and W. J. Nellis, J. Appl. Phys. 52, 3363 (1981).

2. L. V. Al'tshuler, S. B. Kormer, A. A. Bakanova, and R. F. Trunin, Zh. Eksp. Teor. Fiz. 38, 790 (1960) [Sov. Phys. JETP 11, 573 (1960)].

3. S. B. Kormer, A. I. Funtikov, V. D. Urlin, and A. N. Kolesnikova, Zh. Eksp. Teor. Fiz. 42, 686 (1962) [Sov. Phys. JETP 15, 477 (1962)].

4. L. V. Al'tshuler, N. N. Kalitkin. L. V. Kuz'mina, and B. S. Chekin, Zh. Eksp. Teor. Fiz. 72, 317 (1977) [Sov. Phys. JETP 45, 167 (1977)].

5. A. P. Volkov, N. P. Voloshin, A. S. Vladimirov, V. N. Nogin, and V. A. Simonenko, Pis'ma Zh. Eksp. Teor. Fiz. 31, 623 (1980) [JETP Lett. 31, 588 (1980)].

6. C. E. Ragan III, Phys. Rev. A 25, 3360 (1982).

7. C. E. Ragan III, Phys. Rev. A 29, 1391 (1984).

8. A. S. Vladimirov, N. P. Voloshin, V. N. Nogin, A. V. Petrovtsev, and V. A. Simonenko, Pis'ma Zh. Eksp. Teor. Fiz. 39, 69 (1984) [JETP Lett. 39, 82 (1984)].

9. A. C. Mitchell, W. J. Nellis, N. C. Holmes, M. Ross, G. W. Repp, R. A. Heinle, T. C. Valk, J. Rego, W. B. Graham, and R. J. Olness, in Shock Waves in Condensed Matter - 1983, edited by J. R. Asay, R. A. Graham, and G. K. Straub, (North-Holland, Amsterdam, 1984), p. 81.

10. K. S. Trainor, J. Appl. Phys. 54, 2372 (1983) contains a description of the table-generation process for Cu. The Al table is described in K. S. Holian, Los Alamos National Laboratory Report LA-10160-MS, 1984 (unpublished).

11. J. A. Moriarty, D. A. Young, and M. Ross, Phys. Rev. B 30, 578 (1984).

12. F. J. Rogers, Phys. Rev. A 24, 1531 (1981).

13. D. A. Liberman, J. Quant. Spect. Rad. Transfer 27, 335 (1982).

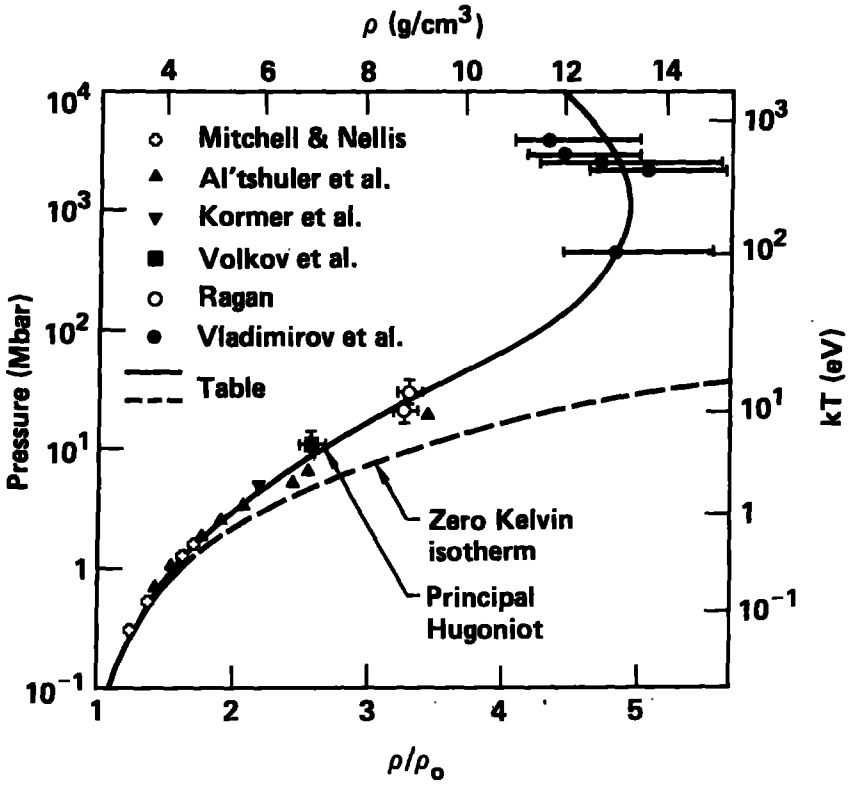


FIG. 1. A comparison of experimental and tabular theoretical shock Hugoniots for Al. Temperatures calculated from the table are indicated, and the 0 K isotherm is also shown for comparison.

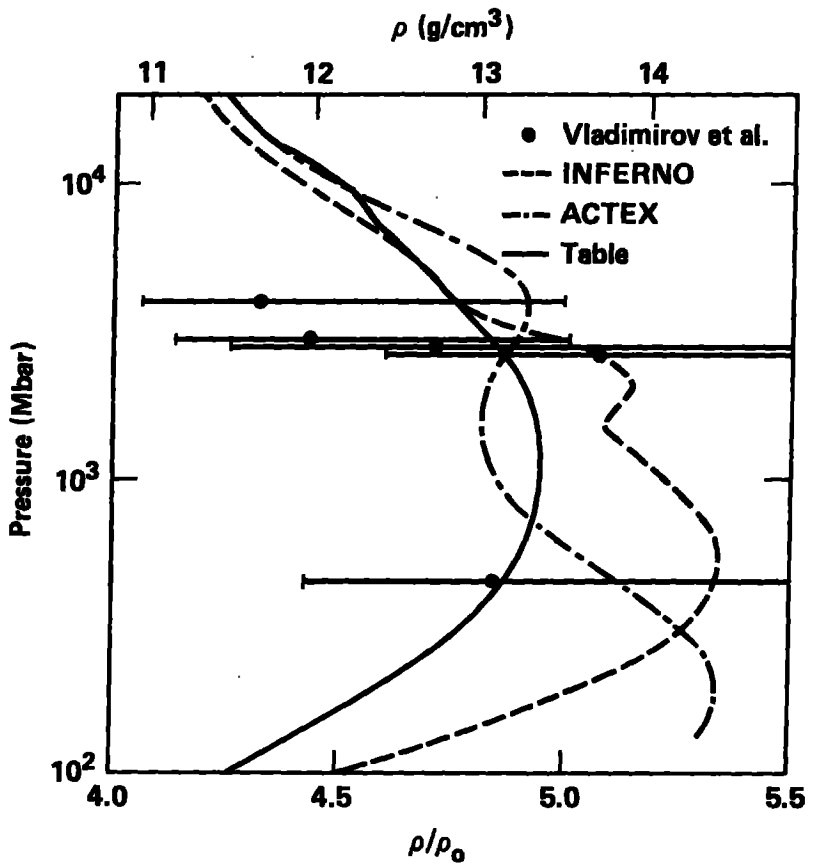


FIG. 2. A detailed comparison of experiment and theory at the highest pressures. The slight cusp in the tabular EOS near $10^4$ Mbar is an artifact of the table boundaries.

# A NEW EOS THEORY OF CLASSICAL EQUILIBRIUM FLUIDS

F. H. Ree

o A new fluid perturbation theory which predicts reliable EOS properties over a wide fluid region is developed. The computational speed and flexibility of dealing with different types of intermolecular potentials allows the new theory to be useful for multi-phase and multi-component chemical equilibrium calculations.

The fluid perturbation theory[1] described below divides the pair potential V(r) into a reference potential $V_0(r)$ and a perturbation potential W(r) at a "break point" $\lambda$ which may depend on density. It also employs a function F(r). This may be expressed in a mathematically rigorous way:

$$V(r) = V_0(r) + W(r) \quad , \tag{1}$$

$$V_0(r) = V(r) - F(r) \quad , \quad \text{if } r \leq \lambda \quad , \tag{2}$$
$$= 0 \quad , \quad \text{if } r > \lambda \quad ,$$

$$W(r) = F(r) \quad , \quad \text{if } r \leq \lambda \quad , \tag{3}$$
$$= V(r) \quad , \quad \text{if } r > \lambda \quad .$$

Here both $\lambda$ and F(r) are arbitrary. However, when these expressions are used in a perturbation theory, the resulting thermodynamic properties will depend on the specific choices of $\lambda$ and F(r). For example, Weeks, Chandler, and Anderson (WCA)[2] assumed $\lambda$ and F(r) to be constant, i.e., $\lambda = r^*$ and $F(r) = V(r^*) = -\epsilon$ [$r^*$ = intermolecular separation at the minimum, $-\epsilon$, of V(r)]. On the other hand, our earlier choice[3] employed $F(r) = V(\lambda)$ and a density- and temperature-dependent $\lambda$, which was determined variationally at fixed temperature (T) and density ($\rho$), to make the Helmholtz free energy insensitive to a small change in $\lambda$.

In this work we use a simpler and more direct approach, i.e.,

$$\lambda = \text{Min}\ (a_{fcc},\ r^*) \quad , \tag{4}$$

where $a_{fcc}$ is the nearest-neighbor distance of the fcc structure,

$$a_{fcc} = 2^{1/6}/\rho^{1/3} \quad . \tag{5}$$

Note that Eq. (4) reduces to the WCA expression ($\lambda = r^*$) at densities below $\rho(r^*)^3 = \sqrt{2}$. At higher densities Eq. (4) is satisfied by $\lambda = a_{fcc}$. This choice is physically reasonable for a dense fluid. At high densities molecules collide predominantly with their nearest neighbors and a stiff repulsion makes a nearest-neighbor pair reaching a separation of $r^*$ [at which $V(r)$ is minimum] highly improbable. Thus a molecule will be essentially confined in a cage formed by the repulsive forces of its neighbors. Under this situation an equilibrium nearest neighbor separation will lie close to $\lambda = a_{fcc}$ rather than to $r^*$. This choice of $\lambda$ makes the range of $V_0(r)$ [Eq. (2)] shrink with density. This is a desirable feature because the corresponding hard-sphere diameter is also reduced and the difficulty of dealing with a metastable hard-sphere fluid does not become serious. Equation (4) also has a computational advantage over the variational determination[3] of $\lambda$, because the calculation is done in a single step rather than by iteration.

As in the case of $\lambda$, $F(r)$ is not unique. WCA made the simplest choice, $F(r) = -\epsilon$, which also works best at the intermediate-to-low density region. We choose here the next simplest form, i.e., a linear function of $r$,

$$F(r) = V(\lambda) - V'(\lambda)\ (\lambda - r) \quad , \tag{6}$$

where $V'(\lambda) = [dV(r)/dr]_{r=\lambda}$ .

The only parameter in the theory is then the hard-sphere (HS) diameter $d$. We use the WCA method of determining $d$, namely,

$$\int d\underset{\sim}{r}\, \{\exp[-\beta V_0(r)] - \exp[-\beta V_{HS}(r/d)]\}\, y_{HS}(r/d) = 0 \quad , \tag{7}$$

where $\beta = 1/kT$ and $y_{HS}(r/d)$ is related to the potential $V_{HS}(r/d)$ and the radial distribution function $g_{HS}(r/d)$ of hard spheres by $g_{HS}(r/d) = \exp[\beta V_{HS}(r/d)]\, y_{HS}(r/d)$.

The excess Helmholtz free energy per particle $A^e$ (with respect to an ideal gas at the same temperature and density) using Eqs. (1) - (7) can be obtained in a perturbation theory similar to the WCA theory, i.e.,

$$A^e = A_{HS} + A_1 \quad . \tag{8}$$

Here the excess free energy $A_0$ of the reference system is accurately given by the hard-sphere excess free energy $A_{HS}$. The first-order perturbation correction $A_1$ under the high-temperature approximation may be expressed as

$$A_1 = \frac{\rho}{2} \int d\underset{\sim}{r}\, W(r) \exp[-\beta V_{HS}(r)] y_{HS}(r/d) \quad . \tag{9}$$

Table 1 compares various theoretical calculations with Monte Carlo simulation results at densities close to the freezing densities of the Lennard-Jones fluid. Deviations of the Ross theory[4] at high density are mainly due to the hard-sphere approximation used to represent the inverse 12th-power fluid. Young and Roger's results[5] without the hard-sphere approximation give improved results at high density and are also listed in Table 1. Note that the WCA theory breaks down at $kT/\epsilon = 20$ and 100. This is due to the absence of a physically reasonable solution for the hard-sphere diameter.[3] The present theory does not have this difficulty because Eq. (4) reduces the size of the hard-sphere diameter, and Eq. (6) optimizes both the reference and the perturbation potentials.

Beside the Lennard-Jones potential, we have also shown that the present formulation gives accurate results for exponential-6, and inverse nth-power fluid ($n \geq 4$) over wide density and temperature ranges. For example, it can predict the pressure of these fluids within 1% of exact simulation results in most cases. These errors are within or only slightly outside the errors in

the simulation results. Since the present theory is not a variational procedure, which is usually the most time-consuming step in calculation of EOS properties when implemented with an appropriate mixture rule, it should be useful in a practical application related to multiphase, multicomponent equilibrium problems involving more than one chemical species, which have been otherwise computationally impractical to carry out until now.

## REFERENCES


1. H. S. Kang, C. S. Lee, T. Ree, and F. H. Ree, J. Chem. Phys. (to appear).

2. J. D. Weeks, D. Chandler, and H. C. Anderson, J. Chem. Phys. 54, 5237 (1971).

3. F. H. Ree, J. Chem. Phys. 64, 4601 (1976).

4. M. Ross, J. Chem. Phys. 71, 1567 (1979).

5. D. A. Young and F. Rogers, J. Chem. Phys. 81, 2789 (1984).

TABLE 1. Pressure (P) and excess internal energy ($U^e$), near the freezing line of the Lennard-Jones fluid, obtained from exact calculation, the present work, and the theories of Ree (Ref. 3), Ross (Ref. 4), WCA (Ref. 2), and Young and Rogers (Ref. 5).

| | | PV/NkT | | | | | | $U^e$/ NkT | | | | | |
|---|---|---|---|---|---|---|---|---|---|---|---|---|---|
| KT/ε | $\rho\sigma^3$ | Exact | This work | Young Rogers | Ross | Ree | WCA | Exact | This work | Young Rogers | Ross | Ree | WCA |
| 2.74 | 1.1 | 10.17 | 10.17 | 10.23 | 10.30 | 10.86 | 10.96 | -1.35 | -1.35 | -1.31 | -1.35 | -1.27 | -1.29 |
| 5 | 1.279 | 13.44 | 13.37 | 13.37 | 13.46 | 14.07 | 15.14 | 0.44 | 0.41 | 0.43 | 0.41 | 0.50 | 0.57 |
| 20 | 1.765 | 16.68 | 16.69 | 16.66 | 16.75 | 17.18 | [a] | 2.65 | 2.65 | 2.65 | 2.65 | 2.77 | a |
| 100 | 2.38 | 14.46 | 14.50 | 14.47 | 14.56 | 14.87 | [a] | 2.89 | 2.90 | 2.89 | 2.91 | 3.00 | a |
| 100 | 2.5 | 16.51 | 16.49 | 16.45 | 16.54 | 16.89 | [a] | 3.37 | 3.37 | 3.35 | 3.37 | 3.47 | a |

[a] No physically reasonable solution exists.

THE STRUCTURE OF DENSE ALKALI HALIDE MELTS

M. Ross and F. J. Rogers

- Calculations of the ion-ion pair distribution functions in shock melted alkali halides show that the melt undergoes a gradual pressure induced structural change from an open NaCl-like structure to one that has a rare gas-like arrangement containing about twelve neighbors of mixed charge.

X-ray scattering and neutron diffraction experiments coupled with Monte Carlo and hypernetted chain (HNC) equation calculations have established that at atmospheric pressure alkali halide melts are characterized by a relatively open NaCl-like structure containing about 5 to 6 atoms in the nearest neighbor shell.[1] The application of pressure is believed to result in a gradual increase in the coordination number, but very little is known experimentally. In the present work, we have used the HNC equation to obtain the pair distribution functions for molten CsI. In addition we have made calculations for several other salts (CsBr, KBr, KCl, NaCL and LiF) at the pressures and temperatures for which shock melting has been reported.[2]

The HNC equation is now widely used for calculating the properties of ionic fluids.[3] The results demonstrate that for realistic potentials the HNC method predicts pair distribution functions that are in good agreement with experiments. HNC calculations were made for the inert gas xenon and for CsI. The xenon results provide a reference against which to judge the occurence of a structural change in CsI to an inert gas-like structure.

The first potential (1) is the simple xenon-like exponential-six (X6) used by Radousky *et al.* to calculate the shock Hugoniot and estimate the CsI freezing curve:

$$\phi_{X6}(r) = \varepsilon \left[\left(\frac{6}{\alpha-6}\right) \exp\left[\alpha\left(1 - \frac{r}{r^*}\right)\right] - \left(\frac{\alpha}{\alpha-6}\right) \left(\frac{r^*}{r}\right)^6\right] , \qquad (1)$$

where $\varepsilon/k$ = 235 K, $\alpha$ = 13.0, $r^*$ = 4.40Å, and k is Boltzmann's constant. The parameters have been chosen to fit the theoretical 0 K CsI isotherm of Aidun et al.[4] The omission of the coulomb term makes it difficult to fit both the low and high pressure part of the isotherm. The present fit is biased toward fitting the high pressure part.

For the second potential (2) we have added a coulomb interaction term to (1):

$$\phi(r) = \phi_{X6}(r) + \frac{Z_1 Z_2 e^2}{r} \quad , \tag{2}$$

where $Z_1$ and $Z_2$ are the ion charges.

Figure 1a shows the partial distribution functions of liquid CsI calculated at its normal melting temperature The atomic separations in the figure are plotted in units of r/a where a is the mean ion sphere radius, or $a = (3V/4\pi/N)^{1/3}$. For these potentials $g_{++} = g_{--}$. The figure exhibits the characteristic alkali halide arrangement of alternating shells of unlike and like charge. Figure 1b compares the total pair distribution function, $g(r) = (g_{++}(r) + g_{+-}(r))/2$, of CsI with that for the xenon-like fluid (potential 1). The figure shows two very different structures. The reader may have noted that there is a shoulder in the first $g_{++}$ peak (see Fig. 2a) near (r/a) = 2.3. This has been previously observed and is the start of a pressure induced splitting into two new peaks.[5]

As the pressure along the freezing line increases the splitting of the $g_{++}$ peak becomes more pronounced. Increasing the pressure from about 300 kbar (3650 K) to near the observed shock freezing point shifts the first $g_{++}$ peak to inside the $g_{+-}$ first peak envelope (Fig. 2a). As a result the total distribution functions of Xe and CsI (Fig. 2b) are now virtually identical. Each ion has about 12 nearest neighbors, as in a close-packed system, of which seven are oppositely charged and five have the same charge. Figure 2a demonstrates that the oppositely charged neighbors on the average approach each other more closely than do ions with the same charge. But a considerable degree of interpenetration exists. At pressures up to 700 kbar no important changes were observed.

These results demonstrate that at sufficiently high density the short range repulsive forces will be dominant over the long range attraction. Figure 3 compares the ratio of the exp-6 contribution to the pressure to that of the Coulomb contribution as a function of volume. Near the pressure of 300 kbar, where the Hugoniot enters the fluid, the contribution of the exp-6 is an order of magnitude larger than that of the Coulomb term. Thus the properties are dominated by the strong repulsive forces and the liquid adopts a xenon or hard sphere-like structure. The application of pressure has the effect of "dialing down" or decoupling the influence of the coulomb forces.

Calculations of the pair-distribution function made for shock melted CsBr (540 kbar and 4650 K), KBr (400 kbar and 4000 K) and KCl (480 kbar and 4100 K) at the pressures and temperatures reported by Kormer show results that are similar to those for CsI. These calculations were made using Tosi-Fumi potentials.[6] In the case of NaCl (700 kbar and 3700 K) the conversion to a dense state is only partially complete. In the case of LiF (2.8 Mbar and 6000 K) only a small change in the structure has occurred.

The present results demonstrate the existence of a gradual pressure-induced shift in the structure of an alkali halide melt from an open NaCl-like arrangement to one characteristic of a simple non-ionic fluid. This effect is caused by the growing dominance of the repulsive forces and is greatest in the larger ions where the Coulomb forces are relatively weaker compared to the repulsive forces. Thus, CsI is a favorable case for further study. The results have important consequences for the theory of melting.

The Lindemann approach to melting takes the view that if we were able to see the melting transition on a microscopic level, we would always see the same scaled picture in the solid. At different temperatures, because of their ability to interpenetrate each other's electronic cores, the atoms will have different effective sizes. However, for a given crystal structure, the ratios of their effective volumes to the total volume of the system will always remain constant at all points along the melting curve, and their relative arrangements in space will always remain the same. Consequently, the pictures along the melting curve will always be identical if properly scaled. This

view of melting does not correspond to the situation in the alkali halides and we conclude that these simple melting laws will not be applicable to these materials.

## REFERENCES


1. Enderby, J. E. and Neilson, G. M., Adv. Phys., 29, (1980) 323.

2. Kormer, S. B., Sov. Phys.-Uspekhi 11, (1968) 229.

3. Dixon, M. and Gillan, M. J., Phil. Mag. B43, (1981) 1099 and Abernathy, G. M., Dixon, M. and Gillan, M. J., Phil. Mag. B43, (1981) 1113.

4. Aidun, J., Bukowinski, M. S. T. and Ross, M., Phys. Rev. B29, (1984) 2611.

5. Dixon, M. and Sangster, M. J. L., J. Phys. C 10, (1977) 301.

6. Tosi, M. P. and Fumi, F. G., J. Phys. Chem. Solids 25, (1964) 45.

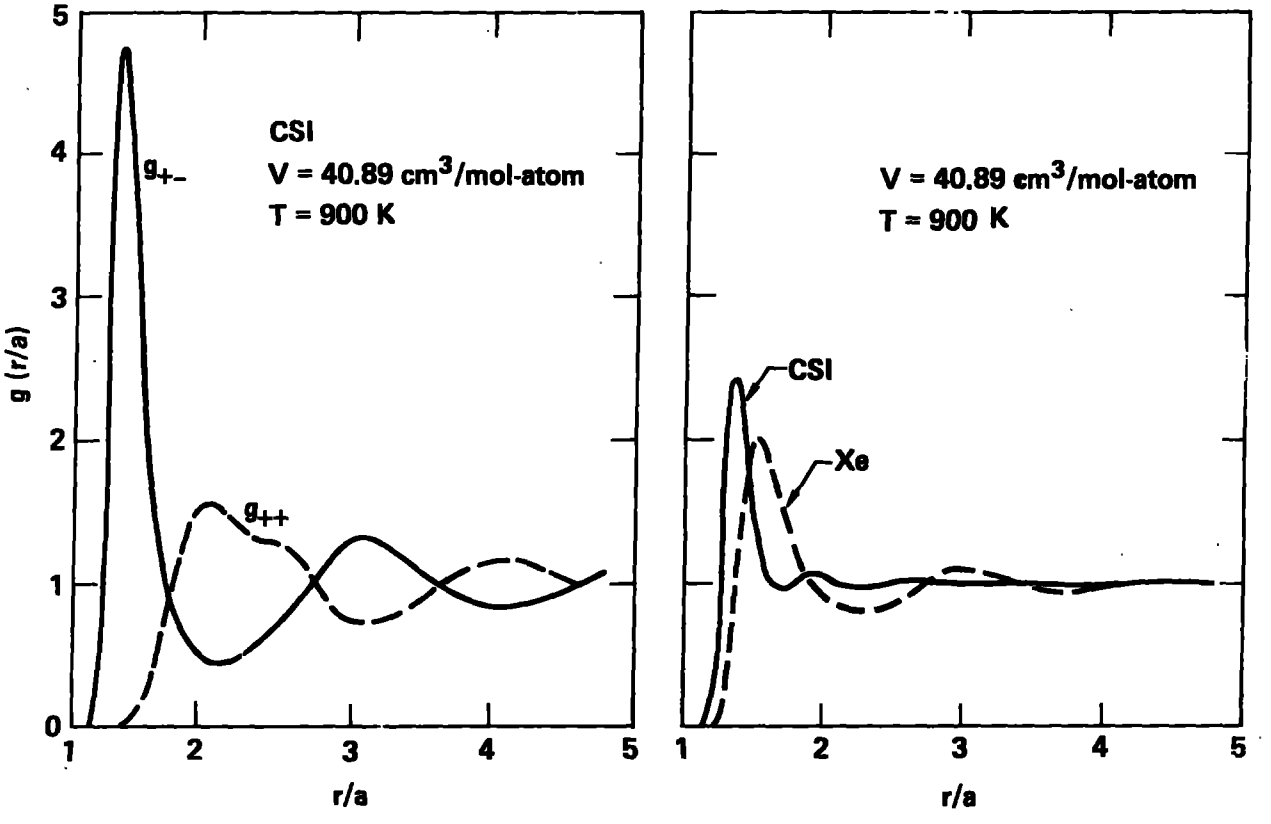


FIG. 1. (a) Partial distribution functions for CsI; (b) Comparison of total distribution functions for CsI and Xe.

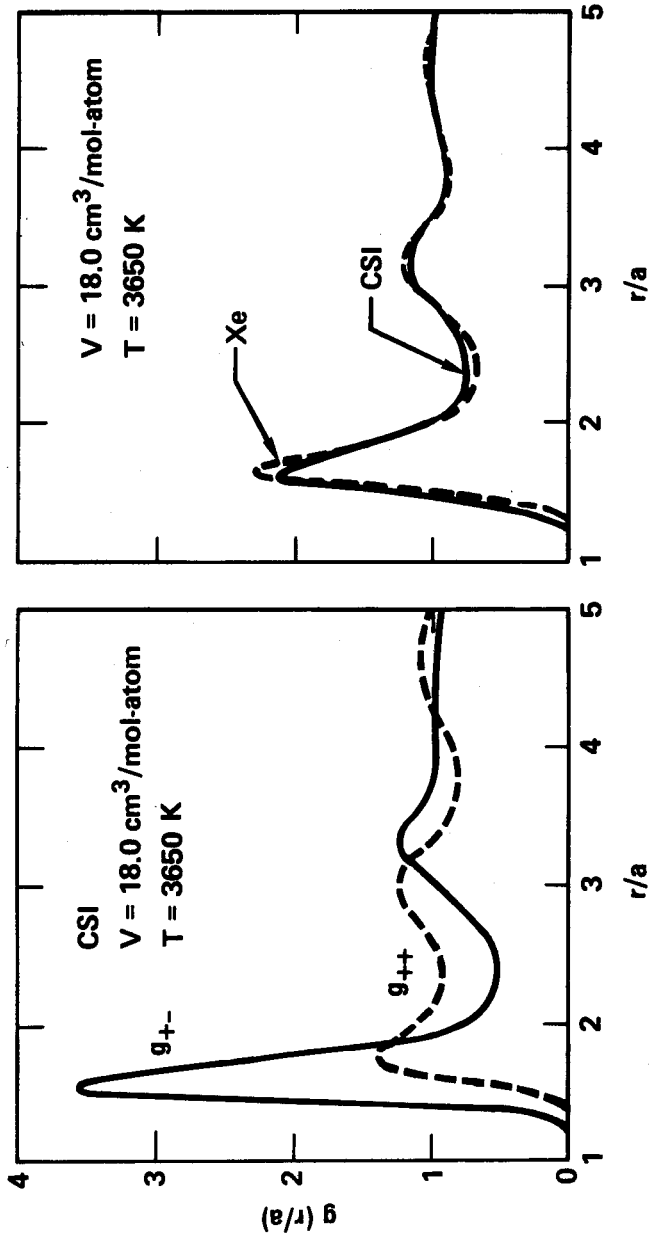


FIG. 2. (a) Partial distribution functions for CsI; (b) Comparison of total distribution functions for CsI and Xe.

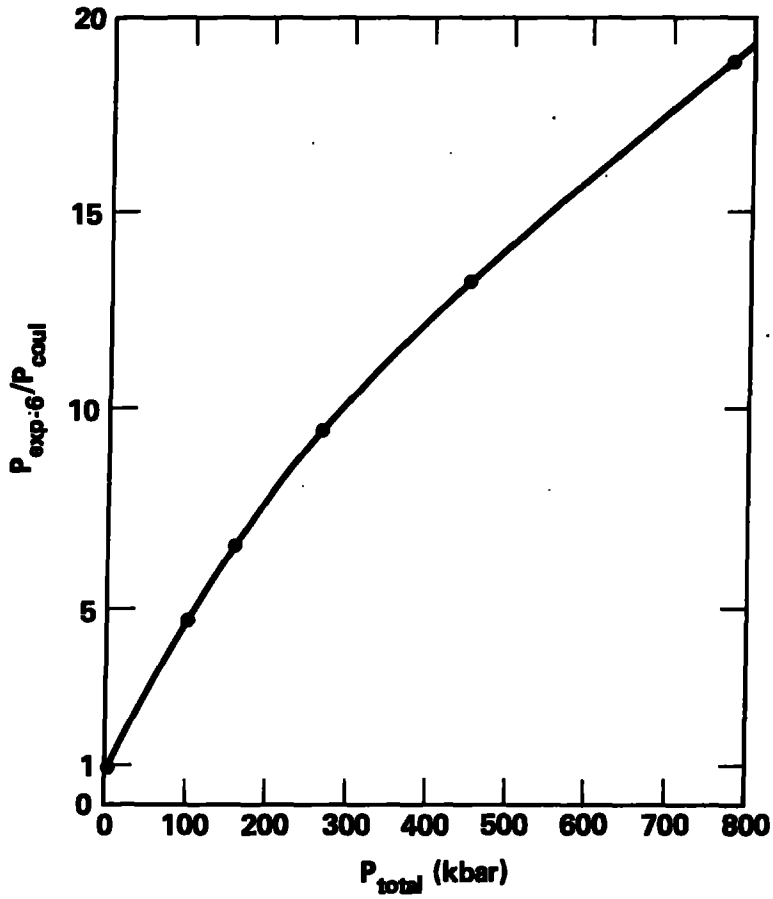


FIG. 3. The ratio of the inert gas contribution of the total pressure to the coulomb contribution as a function of total pressure along the estimated freezing line.

## THE EFFECT OF MATERIAL STRENGTH ON THE RELATIONSHIP BETWEEN THE PRINCIPAL HUGONIOT AND QUASI-ISENTROPE OF BERYLLIUM

W. C. Moss

o Quasi-isentropic [QI] compression can be achieved by loading a specimen with a low strain-rate, long rise time uniaxial strain wave. Recent experimental data show that the quasi-isentrope of 6061-T6 aluminum lies a few percent above the principal Hugoniot, that is, at a given specific volume, the QI stress exceeds the principal Hugoniot stress. It has been suggested that this effect is due to material strength, implying that the QI yield strength can be large. Our calculations show that the QI yield strength is 5.2 GPa in beryllium at a QI stress of 35 GPa.

A method for generating quasi-isentropic [QI] compression waves in flat plate impact (uniaxial strain) experiments has been developed recently by Barker [1]. The QI waves are generated by impacting a specimen with a projectile whose nose-piece has an impedance that increases monotonically from a low value at the impacting surface, to a high value at the back of the nose-piece. The resulting wave has a long rise time, and produces much lower strain-rates in the specimen than shock loading to the same specific volume reached by the QI compression. Although elastic- plastic effects in the specimen make the loading thermodynamically irreversible, much less heat is generated than by shock compression (to the same specific volume), hence, the loading is referred to as quasi-isentropic.

One would expect that at a given specific volume, the principal Hugoniot stress ($\sigma_H$) would be greater (compressive stresses are positive) than the quasi-isentropic stress ($\sigma_{qi}$), due to the increased entropy production in the shock process, but Barker [1] has determined experimentally that the quasi-isentrope of 6061-T6 aluminum is a few percent above the principal Hugoniot, for Hugoniot stresses less than 9 GPa (the range of the data). ($\sigma$ is the longitudinal stress in a uniaxial strain configuration, and is related to the pressure [P] by $\sigma = \sigma' + P$, where $\sigma'$ is the longitudinal deviatoric stress). It has been suggested that this effect is due to material strength.

Figure 1 illustrates schematically the relationship between the stresses, pressures, and deviatoric stresses on the principal Hugoniot and quasi-isentrope. The figure also shows how material strength (values of the deviatoric stresses) can account for $\sigma_{qi}(V)>\sigma_H(V)$. The dashed lines show the Hugoniot stress and pressure. The difference between the two curves is the deviatoric Hugoniot stress $[\sigma'_H(V)]$. The solid lines show the QI stress and pressure. The difference between the two curves is the deviatoric QI stress $[\sigma'_{qi}(V)]$. In the figure $\sigma_{qi}(V)>\sigma_H(V)$, to be consistent with the experimental data for 6061-T6 aluminum. In general, theory places no restriction on the relationship between $\sigma_{qi}$ and $\sigma_H$. $P_{ise}(V)$ [dot-dashed line] is the true isentropic pressure, that is, the pressure resulting from a reversible adiabatic compression. Theory requires $P_{ise}(V)$ to be less than $P_{qi}(V)$, $P_H(V)$, $\sigma_H(V)$, and $\sigma_{qi}(V)$. $P_{qi}(V)$ lies above $P_{ise}(V)$, because the heat produced by plastic work along the quasi-isentrope raises the pressure above the isentropic value. $P_H(V)$ must also lie above $P_{ise}(V)$, due to the heat produced by plastic work and the heat generated by the shock process. It is not known whether $P_H(V)$ exceeds $P_{qi}(V)$, in general, because the amount of plastic work that is done along the quasi-isentrope differs from that along the Hugoniot. Thus, $P_H(V)>P_{qi}(V)$ if the sum of the heat due to plastic work along the Hugoniot and the heat due to the shock process exceeds the heat due to to plastic work along the quasi-isentrope. In the figure, we have chosen arbitrarily to show $P_H(V)>P_{qi}(V)$.

We should emphasize that the difference between the $P_{ise}$, $P_{qi}$, and $P_H$ curves is small; the figure is exaggerated, for clarity of presentation.

We conclude our discussion of the figure by noting that if $\sigma'_{qi}(V)>\sigma'_H(V)$ by a sufficient amount, then $\sigma_{qi}(V)>\sigma_H(V)$.

Figure 2 shows our calculation of $\sigma_{qi}$ (solid line) and $\sigma_H$ (dashed line), as functions of specific volume for beryllium. Experimental Hugoniot data [2] are also shown in the figure. For Hugoniot stresses greater than

8.4 GPa, $\sigma_{qi} > \sigma_H$. The maximum relative difference is 0.023, at V = 0.456 [$\sigma_H$=27.2 GPa] . Our calculation yields $P_H > P_{qi} > P_{ise}$ throughout the range of the data ($0 \leq \sigma_H \leq 35$ GPa). The relative difference between $P_{qi}$ and $P_{ise}$ is negligible. The relative difference between $P_H$ and $P_{qi}$ increases monotonically to 0.01, at V = 0.44 [$\sigma_H$ = 35 GPa] . Material strength is responsible for $\sigma_{qi} > \sigma_H$, because $\sigma'_{qi} \geq \sigma'_H$ throughout the range of the data.[3] If we assume that the calculated values of $\sigma'_{qi}$ for beryllium are underestimates, as they are for aluminum, then the ratio $Y/\sigma_{qi}$ for beryllium could be as large as 0.15 at $\sigma_{qi}$ = 35 GPa.[3] It would be useful to obtain the quasi-isentrope of beryllium experimentally, to check this prediction.

## REFERENCES


1. Barker, L. M., Shock Waves in Condensed Matter - 1983 (Eds., J. R. Asay, R. A. Graham, and G. K. Straub, Amer. Inst. of Physics, New York, 1984) 217.

2. Wise, J. L., L. C. Chhabildas, and J. R. Asay, Shock Waves in Condensed Matter - 1981 (Eds., W. J. Nellis, L. Seaman, and R. A. Graham, Amer. Inst. of Physics, New York, 1982) 417.

3. Moss, W. C., J. Appl. Phys., in press.

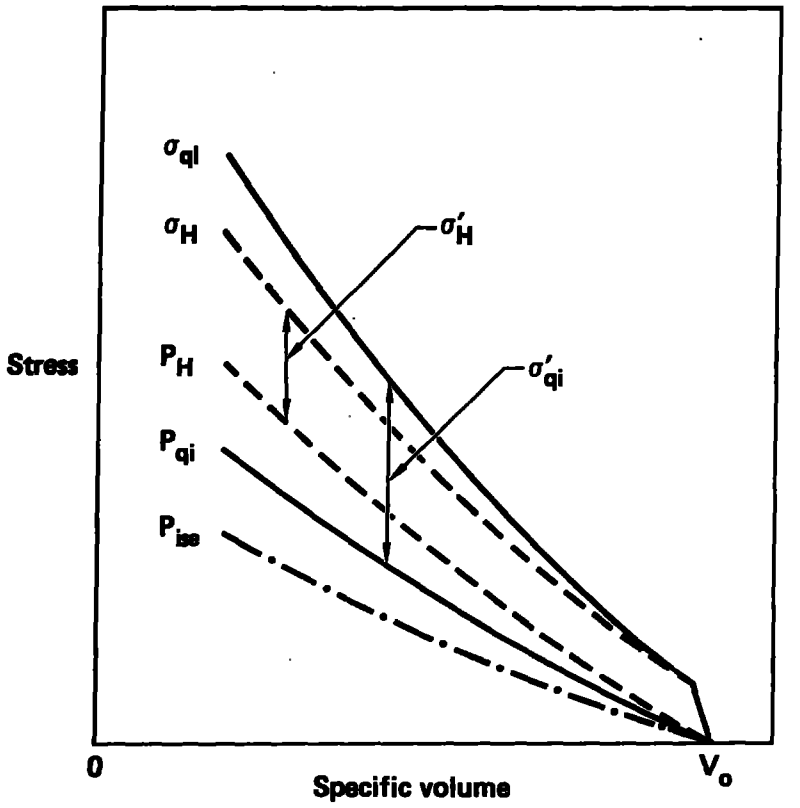


FIG. 1. The relationship between stresses and pressures on the principal Hugoniot and quasi-isentrope.

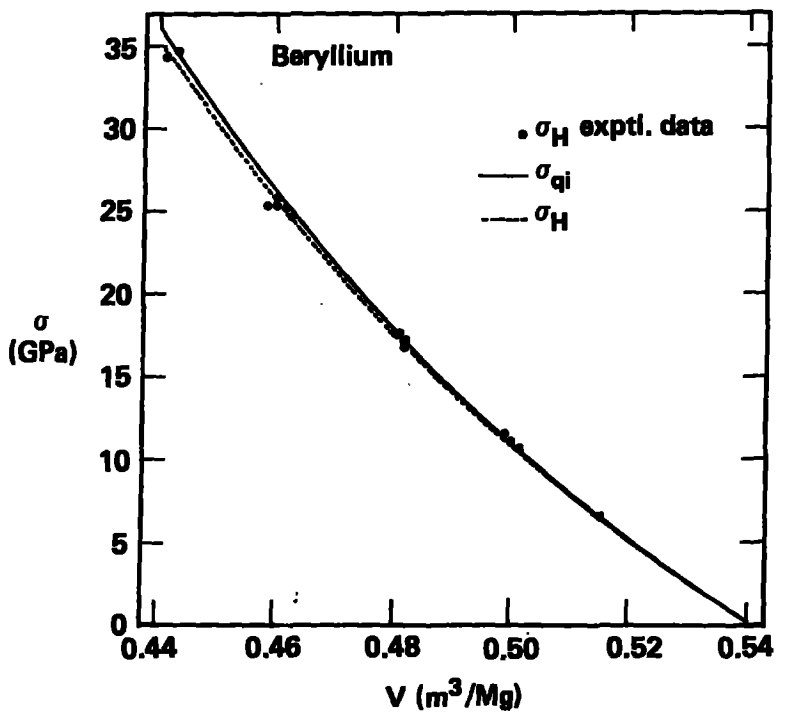


FIG. 2. Calculated principal Hugoniot and quasi-isentrope, and experimental Hugoniot data as functions of specific volume.

## ELASTIC RADIATION FROM EXPLOSIVELY-LOADED ELLIPSOIDAL CAVITIES IN AN UNBOUNDED MEDIUM

L. A. Glenn, A. J. C. Ladd, B. Moran, and K. A. Wilson

o Elastodynamic calculations were made to determine the radiation spectra from explosively-driven ellipsoidal cavities in an unbounded medium. A finite element code was used to compute the displacements on the cavity surface and the integral representation theorem was then invoked to find the displacements in the far field. The method was applied to ellipsoids with 3:1 and 10:1 aspect ratios and the results were compared to the analytic solution for a sphere of equal volume. Both the peak amplitude and the spectrum of the particle velocities were found to be strongly dependent on direction. For example, along the major axis of the 10:1 ellipsoid, the peak amplitude of the radial velocity component is approximately 7.5 times smaller than along the minor axis, and the frequency at which the peak occurs is 4 times smaller. The ellipsoidal cavities were also found to be effective sources of shear wave radiation.

The idea of using a large cavity to muffle the seismic signal from an underground explosion was first proposed 25 years ago at an early conference on the discontinuance of nuclear tests.[1] Calculations were made to show that the strength of the distant seismic signal in an elastic medium is determined primarily by the volume of the cavity created by the explosion. If the explosion is set off in a large (pre-excavated) cavity, then it is the differential increase that determines the signal amplitude. Moreover, if the cavity is just large enough so that its walls suffer only elastic deformation, the distant (low frequency) signal, for a given yield, is minimized and it does not pay to make the cavity any bigger. Inelastic behavior causes increased coupling because the medium, unable to support the applied shear stress, flows and thus undergoes large displacements.

In recent years, the possibility of high-frequency monitoring has been cited as a potential means of neutralizing cavity decoupling (Larson[2], Blandford[3]). Figure 1 illustrates how this might be accomplished. The

spectral variation of the seismic amplitude is schematically illustrated, for a fixed yield, for both tamped and cavity-decoupled explosions. In either case it is observed that only modest changes occur as the angular frequency is increased to the neighborhood of the eigenfrequency, $\omega \approx c/R$, where c is the wave speed and R the elastic radius, after which severe damping occurs. For the cavity-decoupled explosion, this "corner" fequency is based on the cavity radius, $R_D$. For the tamped explosion, the radius, $R_T$, at which the shock wave attenuates to an elastic wave, is much larger. A heuristic explanation for this derives from the fact that the radial momentum increase in a strong explosion is proportional to the square-root of the mass engulfed by the blast wave, which is evidently many times larger when the cavity is initially filled with rock than with air. Thus, even though the amplitude of the tamped explosion is 50 or more times higher for $\omega < \omega_T = c/R_T$, it may be much less in the region $\omega_T < \omega < \omega_D = c/R_D$. The decoupling factor (the amplitude ratio) then decreases substantially in this frequency interval. Initially it was believed that this effect was of little significance since frequencies greater than $\omega_T$ were supposed to be effectively attenuated by the earth. It now appears that this may not be the case, at least in certain geographical regions of importance.

It should be clear from the above discussion that the decoupling factor would not decrease at all, at high frequency, if the radius of the pre-excavated cavity could be enlarged to $R_T$. Even if this were feasible (which, even for modest yields, it is not) the cost would be prohibitive. An alternate approach is to consider aspherical cavities, whose radiation pattern may be asymmetric, with the potential for very small signals within certain solid angles. Since the orientation of a cavity could be optimized with respect to a known and fixed seismic network, such "aimed" cavities would seriously complicate the network siting problem. Moreover, aspherical cavities generate shear waves, making source identification more difficult. They also may be easier to construct, tnus allowing the excavation of much larger volumes. A preliminary geotechnical assessment of such a system has recently been made (Glenn[4]). In the present work we consider the elastic radiation from the simplest aspherical cavity, an ellipsoid. The DYNA2D

finite element code[5,6] was used to calculate the displacements on the cavity surface and the elastodynamic integral representation theorem[7] was then invoked to determine the displacements in the far field. The method was applied to equal-volume ellipsoids, with 3:1 and 10:1 aspect (axis) ratios, and the solutions were compared to that obtained for a sphere of the same volume. Details of the calculational method can be found in Ref. 8.

The main result is that explosively-loaded ellipsoidal cavities generate very different radiation spectra than do spherical cavities of the same volume. When viewed in the direction of the major axis of the ellipsoid, an observer in the far field will measure substantially reduced high-frequency displacements. The actual reduction will depend on the aspect ratio of the ellipsoid. Figure 2 shows that relative to a spherical cavity of the same volume, the amplitude of the peak radial velocity in the direction of the major axis for the 10:1 ellipsoid is reduced by a factor of 3.9, and the peak frequency is reduced by a factor of 2.4. These results are of some importance in the cavity decoupling of underground nuclear explosions since it may be possible to orient similar cavities so as to mitigate, along directions roughly parallel to the long axis, the predicted reduction of the decoupling factor at high frequency.

Of course, it is unlikely that an ellipsoidal geometry would be chosen. Although a 10:1 aspect-ratio ellipsoid may be feasible from a geotechnical standpoint, a more practical solution would probably be a nearly spheroidal central chamber (of dimensions sufficient to maintain elastic wall response) connected to a long tunnel. The tunnel could be aimed in the direction of a known seismic detection station. We speculate that a uni-directional system might behave as a low-pass filter in a (probably narrow) solid angular segment centered on the tunnel axis. The maximum reduction in seismic amplitude and corner frequency that could be achieved is not known at present. We are currently attempting to derive theoretical estimates from calculations with spherocylindrical and multi-spherical sources.

The concept is readily generalized to a system of several tunnels, each pointing at a separate observer station. It might also be useful to have several tunnels in parallel, since their diameter would likely be much smaller than that of the central cavity, or that of a seismically-equivalent single tunnel. The more general problem of the multi-directional system is also considerably more difficult to analyze since the axial symmetry of the source is no longer preserved in this case. This means that the finite element calculation of the surface displacements on the cavity walls would be much more expensive. We are exploring alternate computational means for dealing with more complex (three-dimensional) cavities.

## REFERENCES


1. Latter, A. L. and Bethe, H., 1960. Verbatim Record of the 7th Meeting of Technical Working Group 2, Conference on the Discontinuance of Nuclear Weapon Tests, held in the Palais des Nations, Geneva, Switzerland, December 2, 1959. GEN/DNT/TWG.2/PV.7, January 15, 1960.

2. Larson, D. B., 1979. Spherical wave propagation in elastic media and its application to energy coupling for tamped and decoupled explosions, UCRL-52655, Lawrence Livermore National Laboratory.

3. Blandford, R. R., 1982. Seismic event discrimination, Bull. Seis. Soc. Am., 72, S69-S87.

4. Glenn, L. A., 1984. Cavity decoupling and the evasion of a comprehensive test ban, J. Geophys. Res. (submitted for publication), UCRL-90321.

5. Hallquist, J. O., 1978. DYNA2D - an explicit finite element and finite difference code for axisymmetric and plane strain calculations, UCRL-52429.

6. Hallquist, J. O., 1982. User's manual for DYNA2D - an explicit two-dimensional hydrodynamic finite element code with interactive rezoning, UCID-18756 Rev. 1.

7. Eringen, A. C. and Suhubi, E. S., 1975. Elastodynamics, Vol. II (Linear Theory), Academic Press, pp. 422-435.

8. Glenn, L. A., Ladd, A. J. C., Moran, B. and Wilson, K. A., 1984. Elastic radiation from explosively-loaded ellipsoidal cavities in an unbounded medium, Geophys. J. (in press), UCRL-91246.

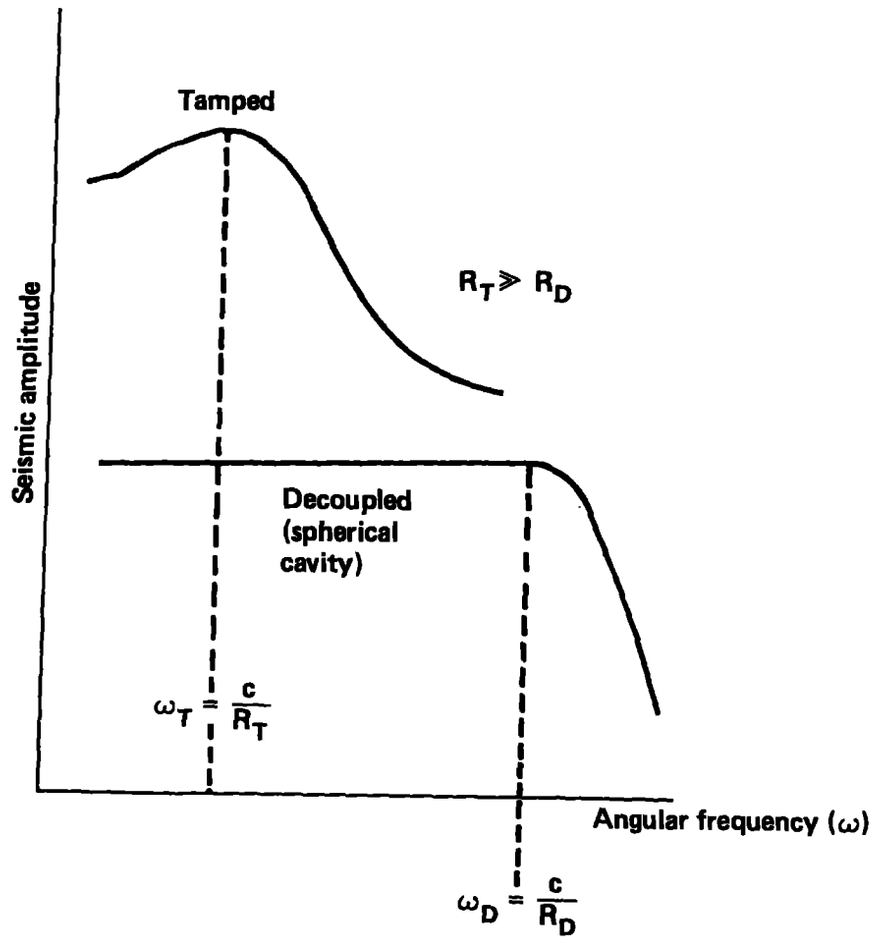


FIG. 1. Spectral variation of seismic amplitude (reduced velocity potential) for tamped and cavity-decoupled explosions. Both abscissa and ordinate scales are logarithmic. The ratio of the tamped to the decoupled amplitude is called the decoupling factor and theoretically decreases at angular frequencies above $\omega_T$.

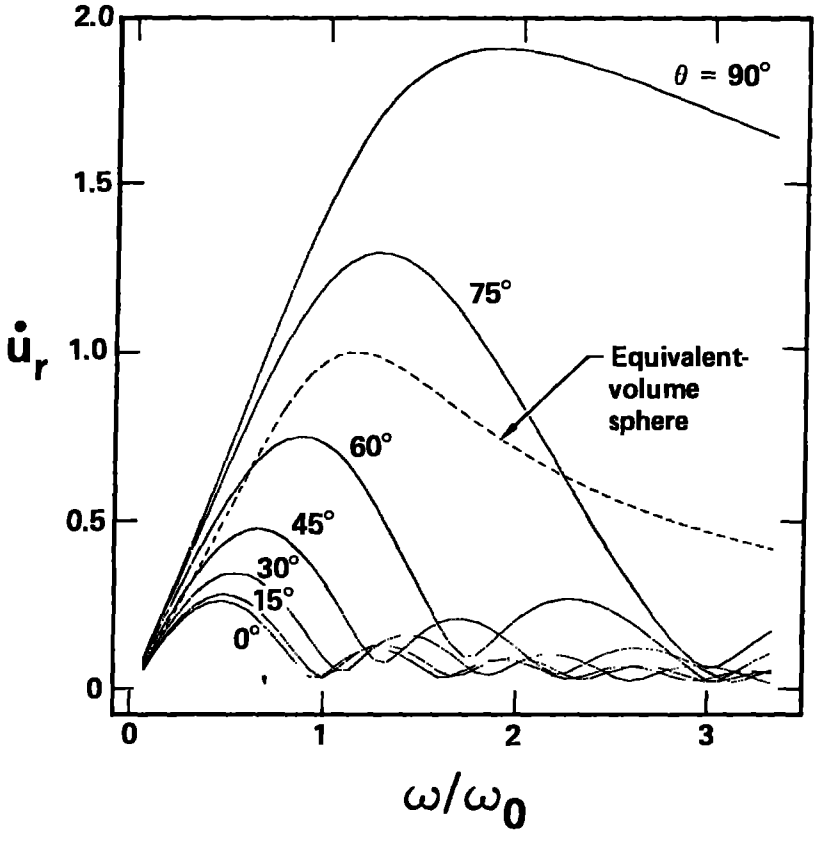


FIG. 2. Spectral variation of the radial particle velocity component, $\dot{u}_r$, as a function of the orientation angle, $\theta$, for the 10:1-aspect-ratio ellipsoid. The data are normalized to the peak value for an equivalent-volume sphere. $\theta = 0°$ is the direction of the major axis. $\omega_0 = C_L/R_0$, where $R_0$ is the spherical radius and $C_L$ is the dilational wave speed.